Liège University

Département d'Astrophysique, Géophysique et Océanographie
Institut D'Astrophysique et Géophysique

Astrophysics

Innovative techniques to find strongly lensed systems

Laisney Clément

1. Reviewer Sluse Dominique
Origines Cosmologiques et Astrophysique
Liège University

2. Reviewer Delchambre Ludovic
Groupe d'AstroPhysique et des Hautes Energies
Liège University

Supervisors Sluse Dominique and Delchambre Ludovic

June 2023

Abstract

Acknowledgement

Contents

1 Introduction **1**
1.1 Physics of Gravitational lenses 2
1.1.1 The Refraction analogy 2
1.1.2 The lens equation 4
1.1.3 Einstein Ring 5
1.1.4 Images positions 6
1.1.5 Magnification 7
1.2 Scientific context 8
1.3 Convolutional Neural Network to the rescue 9
1.4 A new approach 10

2 Data **11**
2.1 Origin of the Data 11
2.2 Exploration of the dataset 13
2.3 Noise and signal 16

Bibliography **21**

A Example Appendix **29**
A.1 Appendix Section 1 29
A.2 Appendix Section 2 29

Declaration **33**

1 Introduction

A gravitational lens, also known as cosmic mirage, is a distribution of mass able to bend the light coming from a distant source. This phenomenon is similar to a light beam bended through a lens by refraction. This is why we call it gravitational lensing.

Already in 1704, Isaac Newton speculated that "[...] Bodies act upon Light at a distance, and by their action bend its Rays; and [...] this action [is] strongest at the least distance." [1]. Later John Mitchell proposed to Henry Cavendish, a method to measure the mass of stars by detecting a reduction of the speed of light affected by gravity [2]. In those letters, Mitchell suggested that a massive enough body could stop the light: a black hole. This pushed Cavendish to calculate the Newtonian light deflection. Unfortunately he never published his manuscript dated around 1784 [3]. Johann Georg von Soldner published the same result in 1801 [4] assuming light is a corpuscule. Finally, Einstein calculated the same value thanks to the equivalence principle only in 1911 [5], and corrected it by twice the value in 1915 [6] in the frame of General Relativity.

The first observation of light deflection were perform in 1919 by Arthur Eddington and Frank Watson Dyson by observing a change in position of stars near the sun during the solar eclipse of May 29 [7]. Later in 1937, after the new discovery of Galaxies, Fritz Zwicky speculate that those massive objects could act as both source and lens with a larger effect much likely to be observed [8]. It was necessary to wait 1979 to observe the first gravitational lens. Dennis Walsh, Bob Carswell and Ray Weysmann observed two identical Quasistellar objects (QSO) using Kitt Peak National Observatory. Their paper [9] arise difficulties in describing them as two distinct objects and the hint of the observation of two images of the same object formed by gravitational lensing is discussed. SBS 0957+561 was renamed "Twin QSO".

1.1 Physics of Gravitational lenses

1.1.1 The Refraction analogy

As said earlier, J. von Soldner calculated the deviation angle of light by a spherical mass M thanks to Newton's theory of gravitation. This deviation angle $\alpha = \frac{2GM}{c^2 b}$ (where G is the gravitational constant, c the speed of light, and b the impact parameter.) was corrected later by Einstein thanks to general relativity. In this part, we will study gravitational lenses in the frame of General relativity.

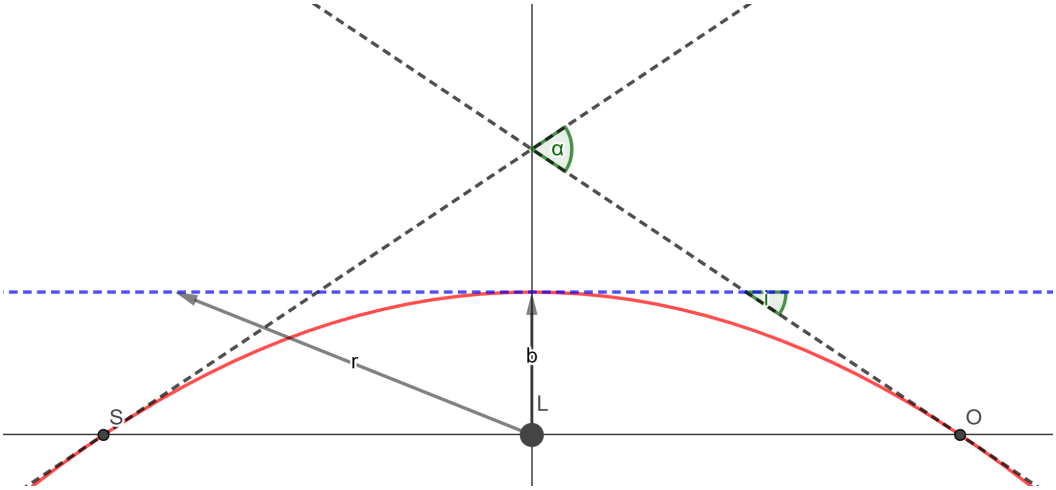

Fig. 1.1.: Deflection of light coming from a distant source (S) in the vicinity of a massive object (Lens: L) seen by the observer (O).

Gravitational mirages are analogs of atmospheric mirages. This phenomenon arises when light trajectories are curved which is a consequence of an anisotropic speed of light along the light path. According to refraction laws, light rays are bent in an inhomogeneous medium. This is why we can approach this problem as a refraction problem, with light traveling from vacuum to a material medium of refraction index n_ϕ.

In vacuum; the speed of light is c, but in a material medium it becomes $v = \frac{c}{n_\phi}$. As a consequence of General relativity, spacetime is curved by a gravitational potential ϕ associated with a massive object. In the weak field approximation $\frac{\phi}{c^2} \ll 1$ and the metric is :

$$ds^2 = -\left(1 + \frac{2\phi}{c^2}\right) c^2 dt^2 + \left(1 - \frac{2\phi}{c^2}\right) (dx^2 + dy^2 + dz^2) \tag{1.1}$$

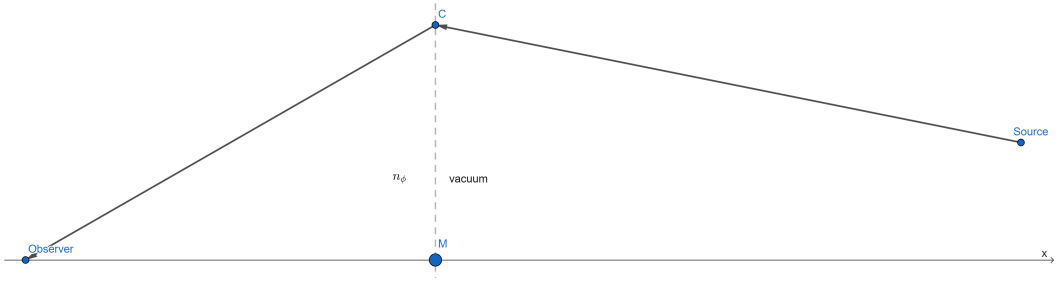

Fig. 1.2.: Analog situation of light traveling in vacuum from a distant source and propagating through a medium of refraction index n_ϕ.

By tacking the null geodesic corresponding to the light path and $\frac{1}{1+\frac{2\phi}{c^2}} \approx 1 - \frac{2\phi}{c^2}$ with $\frac{2\phi}{c^2} \ll 1$:

$$ds^2 = 0 \tag{1.2}$$

$$\left(1 + \frac{2\phi}{c^2}\right) c^2 dt^2 = \left(1 - \frac{2\phi}{c^2}\right) (dx^2 + dy^2 + dz^2) \tag{1.3}$$

$$dt^2 = \frac{1 - \frac{2\phi}{c^2}}{1 + \frac{2\phi}{c^2}} \frac{(dx^2 + dy^2 + dz^2)}{c^2} \tag{1.4}$$

$$dt^2 = \left(1 - \frac{2\phi}{c^2}\right)^2 \frac{(dx^2 + dy^2 + dz^2)}{c^2} \tag{1.5}$$

$$dt = \left(1 - \frac{2\phi}{c^2}\right) \frac{\sqrt{dx^2 + dy^2 + dz^2}}{c} \tag{1.6}$$

$$\frac{\sqrt{dx^2 + dy^2 + dz^2}}{dt} = \frac{c}{\left(1 - \frac{2\phi}{c^2}\right)} \tag{1.7}$$

equation 1.7 is analog to $v = \frac{c}{n_\phi}$. We identify $n_\phi = 1 - \frac{2\phi}{c^2}$. That being said, let's establish the lens equation and the deflection angle.

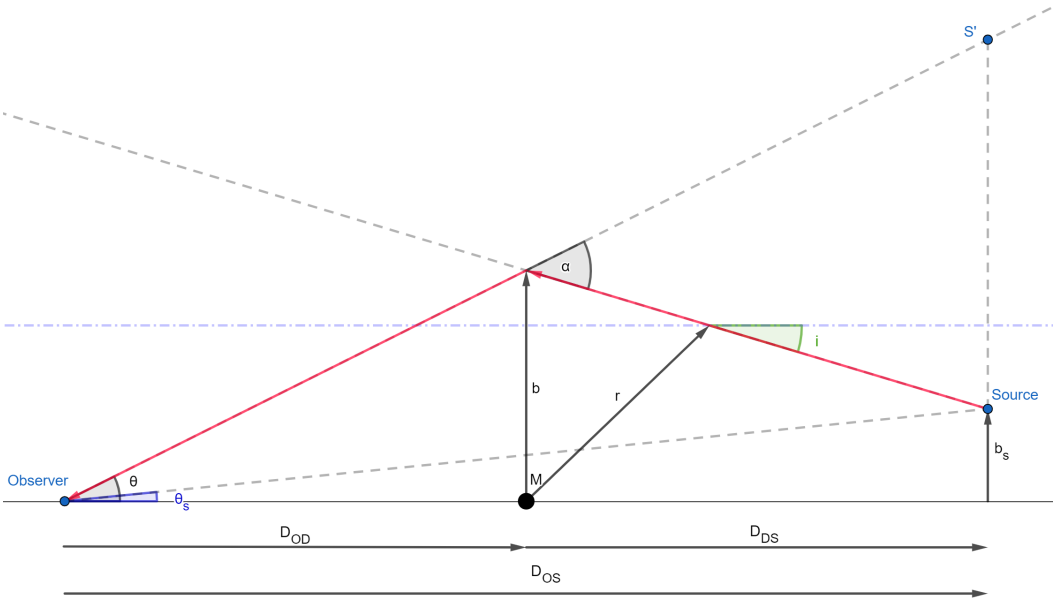

Fig. 1.3.: Scheme of the general situation of a gravitational lens

1.1.2 The lens equation

To solve this problem we need to link the viewing angle θ to the deflection angle α. By geometric considerations thanks to figure 1.3 this relation is given by the following equation :

$$\theta_s = \theta - \frac{D_{DS}}{D_{OS}}\alpha(b) \tag{1.8}$$

$$b = D_{OD}\theta \tag{1.9}$$

Now we have to link the deflection angle α to physical parameters like the mass of the deflector M. In the following, $\frac{di}{dx}$ is the variation of the direction along x axis. α is thus the deflection angle which is the integration of all direction variation along x.

$$\overrightarrow{\alpha}(b) = -\int_{-} \frac{d\overrightarrow{i}}{dx}dx = -\int_{-} \frac{1}{n}\overrightarrow{\nabla_b} n dx = \frac{2}{c^2}\int_{-} \overrightarrow{\nabla_b}\phi dx \tag{1.10}$$

In this demonstration we will take as simple example a point mass deflector. It's gravitational potential is :

$$\phi = -\frac{GM}{r} = -\frac{GM}{\sqrt{b^2 + x^2}} \tag{1.11}$$

The deflection angle α becomes:

$$\vec{\alpha}(b) = \frac{4GM}{c^2 b^2}\vec{b} \tag{1.12}$$

We effectively find twice the value obtained with the Newtonian framework. Now that we find what Einstein predicted, let's generalize. To do so, we use the thin lens approximation. This approximation allows us to describe a deflector by its surface mass density $\Sigma(\vec{b})$ projected in the deflector plane. The deflection angle is then expressed :

$$\vec{\alpha}(b) = \frac{4G}{c^2}\int_S \frac{\Sigma(\vec{b'})(\vec{b} - \vec{b'})db'_1 db'_2}{|b - b'|^2} \tag{1.13}$$

In the case of a circularly symmetric mass distribution, with $M(b)$ the mass inside a the radius b:

$$\vec{\alpha}(b) = \frac{4GM(b)}{c^2 b^2}\vec{b} \tag{1.14}$$

1.1.3 Einstein Ring

Let's now assume the following circularly symmetric lens mass distribution:

$$M(b) = M_0\left(\frac{b}{b_0}\right)^{\beta} \tag{1.15}$$

$\beta = 0$ correspond to a point mass distribution, $\beta = 1$ is the singular isothermal sphere distribution and $\beta = 2$ yield the uniform distribution of matter.

Now that we have the general case, let's study a particular case which is the Einstein ring solution. This case correspond to the simple case when the observer, the deflector and the source are aligned ($\theta_s = 0$). The Einstein ring is thus defined by its angular size θ_E.

$$0 = \theta_E - \frac{D_{DS}}{D_{OS}}\frac{4GM(b)}{c^2 b} = \theta_E - \frac{D_{DS}}{D_{OS}}\frac{4G}{c^2 b}M_0\left(\frac{b}{b_0}\right)^{\beta} \tag{1.16}$$

$$0 = \theta_E - \frac{D_{DS}}{D_{OS}}\frac{4GM_0}{c^2 b_0^{\beta}}\left(D_{OD}\theta_E\right)^{\beta-1} = \theta_E\left(1 - \frac{D_{DS}}{D_{OS}}\frac{4GM_0}{c^2 b_0^{\beta}}D_{OD}^{\beta-1}\theta_E^{\beta-2}\right) \tag{1.17}$$

$\theta_E = 0$ is a solution but not relevant.

$$\frac{D_{DS}D_{OD}^{\beta-1}}{D_{OS}}\frac{4GM_0}{c^2 b_0^{\beta}}\theta_E^{\beta-2} = 1 \tag{1.18}$$

$$\theta_E = \left(\frac{4GM_0}{c^2 b_0^{\beta}}\frac{D_{DS}}{D_{OD}^{1-\beta}D_{OS}}\right)^{\frac{1}{2-\beta}} \tag{1.19}$$

with M_E the mass inside the radius $b_E = D_{OD}\theta_E$ we get the expression of the Einstein ring angular size:

$$\theta_E = \sqrt{\frac{4GM_E}{c^2}\frac{D_{DS}}{D_{OD}D_{OS}}} \tag{1.20}$$

1.1.4 Images positions

By tacking a point mass deflector case ($M(b) = M_0$):

$$\theta_s = \theta - \frac{D_{DS}}{D_{OS}}\frac{4GM_0}{c^2 b} = \theta - \frac{D_{DS}}{D_{OS}}\frac{4GM_0}{c^2 D_{OD}\theta} \tag{1.21}$$

$$\theta\theta_s = \theta^2 - \frac{D_{DS}}{D_{OS}D_{OD}}\frac{4GM_0}{c^2} \tag{1.22}$$

with $M_E = M_0$

$$\theta^2 - \theta_s\theta - \theta_E^2 = 0 \tag{1.23}$$

we are in presence of a second order polynom with a determinant $\delta = \theta_s^2 + 4\theta_E^2 > 0$ and its two solutions:

$$\theta_{1,2} = \frac{1}{2}\left(\theta_s \pm \sqrt{\theta_s^2 + 4\theta_E^2}\right) \tag{1.24}$$

Let's now study two interesting properties. By considering a small misalignment ϵ between the source, the lens and the observer; at first order the angular separation of the image $\Delta\theta$ is:

$$\theta_1 = \frac{1}{2}\left(\epsilon + \sqrt{\epsilon^2 + 4\theta_E^2}\right) = \frac{1}{2}\epsilon + \frac{1}{2}\sqrt{4\theta_E^2} = \frac{1}{2}\epsilon + \theta_E \tag{1.25}$$

$$\theta_2 = \frac{1}{2} - \theta_E \tag{1.26}$$

$$\Delta\theta = \theta_1 - \theta_2 = 2\theta_E \tag{1.27}$$

This means that the angular separation between 2 images increases with the mass of the deflector or increases when the deflector is closer to the observer.

The second property is about the mean surface density within θ_E which remains constant. We define this quantity as the critical surface mass density:

$$\bar{\Sigma}(\theta_E) \equiv \frac{M_E}{\pi(D_{OD}\theta_E)^2} = \frac{c^2 D_{OS}}{4\pi G D_{OD} D_{DS}} \equiv \Sigma_{crit} \tag{1.28}$$

This property implies that a finite massive object is a gravitational lens which produces multiple images if its central mass density $\Sigma > \Sigma_{crit}$

1.1.5 Magnification

Another property of gravitational lenses is the magnification. This quantity μ is given by the ratio between surface brightness of the image and the source. In the following we will stay in a 1D case but the magnification can be generalized using Jacobian given by this definition:

$$\mu = \frac{d\Omega_{image}}{d\Omega_{source}} = \left| det\left(\frac{\partial \theta_s}{\partial \theta}\right)\right|^{-1} \tag{1.29}$$

Assuming a circular symmetry of the lens as in the figure 1.4: $\mu = \frac{\theta}{\theta_s}\frac{d\theta}{d\theta_s}$

by considering $u = \frac{\theta_s}{\theta_E}$ the lens-image separation in units of Einstein ring radius, we get:

$$\mu_{\pm} = \frac{u^2+2}{2u\sqrt{u^2+4}} \pm \frac{1}{2} \tag{1.30}$$

The $+$ solution is always magnified while the $-$ solution can be magnified or demagnified depending on the value of u. If the source is inside the Einstein radius, $\mu > 1.34$.

Finally, the total magnification gives:

$$\mu = \mu_+ + \mu_- = \frac{u^2+2}{u\sqrt{u^2+4}} > 1 \tag{1.31}$$

For a point-like source, if $u \to 0$, $\mu \to \infty$. If $u \to \infty$, $\mu \to 1$. In the case of a too small image separation, the magnification can still be measured. This is used when the mass of the deflector is to small and this technique is called micro-lensing.

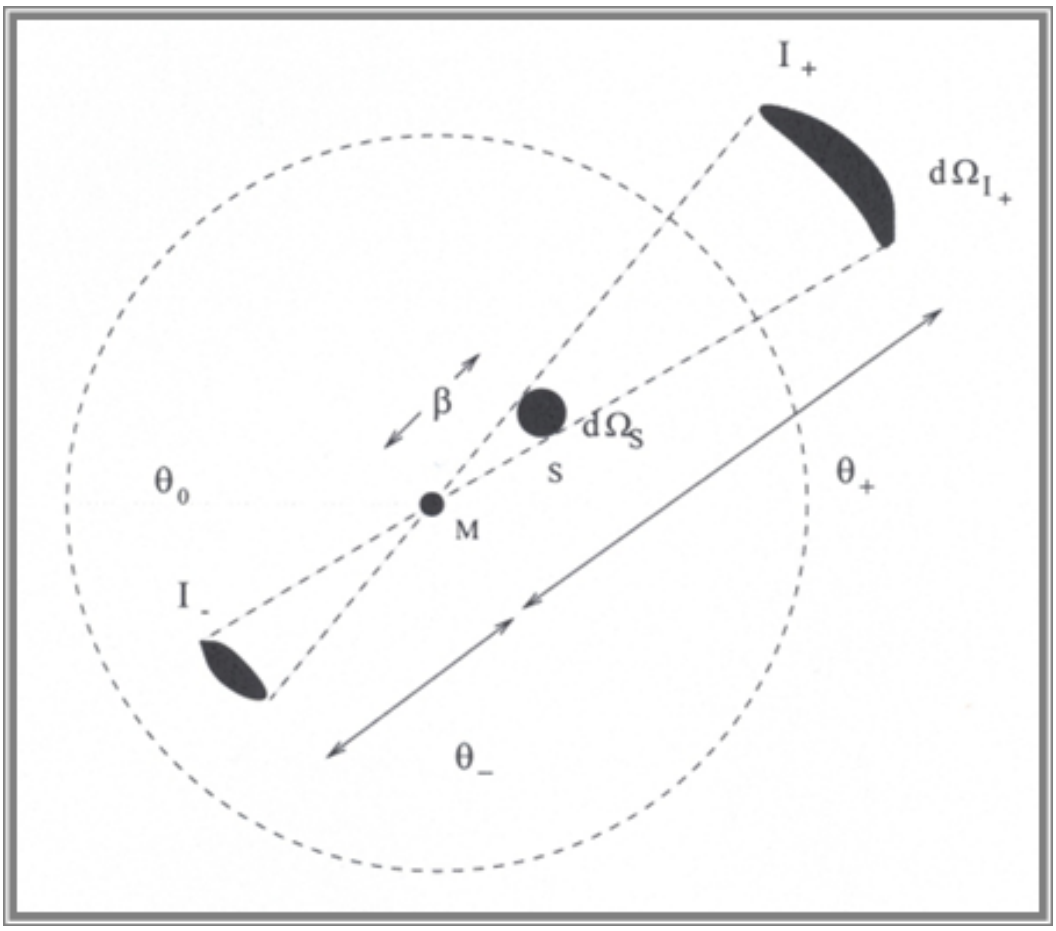

Fig. 1.4.: Illustration of a gravitational lens with magnification. β correspond to the angle between deflector and source which is θ_s in the previous demonstration.θ_- and θ_+ are respectively the demagnified and magnified images positions. The dotted circle correspond to the Einstein ring position.

1.2 Scientific context

Lenses used to be serendipitously found; but nowadays we are looking for gravitational lenses in large amount thanks to large survey programs. One can cite the Cosmic Lens All-Sky Survey (CLASS) which was one of the first survey dedicated to gravitational lenses. Twenty two lensed systems were found using the Very Large Array (VLA) radio telescope [10].

We generally subdivide lensing in 3 categories: Strong, Weak and Micro-lensing. The strong lensing is the case where a distortion of the background source is clearly identified. For a weak lensing, distortion is much smaller and statistical studies are needed in order to find distortion of about few percents. The micro lensing does not show any distortion but a variation of the background source light. The

lensing object in a micro lensing case may be a star while strong and weak lenses are typically galaxies or even galaxy clusters. Micro lensing is ofen used to detect exoplanets [11]. In this work, I will focus on strongly lensed systems.

Studying gravitational lenses has a huge scientific interest. As F. Zwicky already mentioned in his paper in 1937 [8], they constitute a good source to test general relativity, they enable us to observe very distant galaxies and they allow us to determine masses of galaxies. In fact, it has many more applications like the determination of cosmological parameters (Ω_0: density parameter, λ_0: cosmological constant, and H_0: the Hubble constant).

With the rise of Large surveys and their ability to store a large amount of data, we are facing Big Data problems. Processing this tremendous amount of data by hand is just impossible. In addition, the Euclid spacecraft will be soon launched and will provide more data with stunning quality. This is why it is important to detect lensed systems autonomously. The strategy adopted today is the rise of candidates from data to be followed up later with ground-based telescopes.

1.3 Convolutional Neural Network to the rescue

With the era of surveys, Astrophysics has to deal with a huge amount of data and faces similar problems as the Big Data industry. As the amount of data grows, Machine learning and Deep learning field improved in the same time allowing the industry to struggle the processing of those data.

The main type of data in Astrophysics is images and this is especially the case for the study of gravitational lenses. Automatically detecting gravitational lenses require methods able to detect localized features. Convolutional Neural Networks (CNN) are well-suited for this task. Convolution layers are able to detect local correlation with features learned from the data.

CNNs have proven their efficiencies in many fields as computer vision and self-driven cars but also in research field like medicine and biology. This is why so many attempt of auto detection of gravitational lenses uses CNNs. Obviously there are other methods investigated but CNNs are widely at the core of the studies [12][13][14].

In this work we will use the same data as E. Savary, K. Rojas, M. Maus, et al. [14] but we will use a different method. We will then be able to compare the results of

these two methods. This article [14] mainly use a pre-trained CNN available in the `Keras API`: EfficientNet [1].

1.4 A new approach

This work aims to explore innovative techniques to automate the detection of gravitational lenses. As mentioned earlier, we will exploit data from E. Savary, K. Rojas, M. Maus, et al.[14]. We will mainly deeply explore one method but we will later discuss different ones.

Using a CNN based algorithm, results in a loss of interpretability. Indeed, Neural networks are often considered as black boxes even if we succeed to intuitively understand what is going on inside of this black box. In this master thesis we will mostly discuss parametric models mainly based on the Sersic model [15].

The principle of this work is to fit a Sersic model and/or a set of different indices on the candidate and discriminate the presence of a lens thanks to them. To well understand the idea of the method, let's only consider a sersic model. The sersic profil is mainly defined by 3 parameters : the amplitude I_e, the effective radius R_e and the sersic index n: $I(R) = I_e exp\left(-b_n\left[\left(\frac{R}{R_e}\right)^{\frac{1}{n}} - 1\right]\right)$. for a typical profile we barely know the values of those 3 parameters; in case a gravitational lens is present, the luminosity in the arms of the galaxy will increase and this three indices will also be modified: a larger effective radius and a less picky profile which means a larger value of n. In the parameter space we should observe a separation of clouds allowing us to discriminate non-lensed from lensed galaxies. The same logic will be applied with many more parameters.

In this report we will start by describing data: How was it built ? what's the signal nature ? and Which statistics can we use ? In a second time we will focus on the methods used to perform this work: Which kind of algorithm ? Which choices I made ? Does this method more efficient than the CNN method ? And before a conclusion we will discuss our results and the other methods we could have use.

[1] `https://keras.io/api/applications/efficientnet/`

2 Data

As said earlier, data comes from E. Savary, K. Rojas, M. Maus, et al.[14] and a good start is to have a wide knowledge of the dataset. The first step is to know how was collected those data. The second step is to make a sanity check of the dataset and identify the different possible case present in the data. And the last step is to identify the nature of the signal and the associated statistics.

2.1 Origin of the Data

CFIS stands for Canada France Imaging Survey, which is a component of the Ultraviolet Near Infrared Optical Northern Survey (UNIONS). UNIONS is a Collaboration open to Canadian, French, Japanese PhD student and astronomers and the member of the Pan-STARRS team as well. This collaboration aims to provide answers about dark matter, galactic to cluster scaled structures of the Universe and the assembly of the Milkyway. This collaboration will contribute to ground-based photometry within the Euclid ESA space mission[1].

CFIS mainly uses the Canada-France-Hawaii Telescope (CFHT) to complete a survey of 8000 deg^2 of the northern sky in the u photometric band (CFIS-u) and 4800 deg^2 in the r photometric band (CFIS-r). CFHT is a world-class 3.6 m optical/infrared telescope located on top of the Mauna Kea volcano in Hawaii[2](4200m above sea level). It is equiped of MegaCam which is a wide field optical imaging device built from 40 2048x4612 pixels CCD cells. MegaCam has a total of 380 Megapixels for a square Field-of-View (FoV) of 1 deg^2. The resolution of the telescope is 0.187 arcsecond/pixel.[3]

The dataset we are using is simulated images from real data coming from the CFIS Data Release 2 and HST/ACS F814W images. The way it is built is the following: CFIS images are used as deflectors galaxies and Hubble Space Telescope (HST) images lie in background sources. Images size is a square of 44 pixels which

[1] https://www.skysurvey.cc/
[2] https://www.cfht.hawaii.edu/en/about/
[3] https://www.cfht.hawaii.edu/Science/CFIS/

represent a FoV of 8.17". Images from CFIS are exclusively from CFIS-r data and more specifically Luminous Red Galaxies (LRG). These objects are expected to have the largest lensing cross section due to their bright and massive properties. Background galaxies were converted in the r photometric band with HSC ultra-deep stacked images. Images have a FoV of 10" for each side which corresponds to 0.03" per pixels.

In this work, like in the reference paper, we will perform a classification and thus train classifiers to identify gravitational lenses. To do so we need positive cases and negative cases. Negative cases is just a random sample from the CFIS data, but positive cases are build from scratch. The main steps of the design of positive cases follows this main steps:

- Random selection of a LRG
- Association of a singular isothermal ellipsoid model (Assumption)
- Random selection of a galaxy from HST sample
- Position of the source is randomly chosen with magnification $\mu \geq 2$
- Computation of high resolution images of the lensed source
- Convolution of the lensed source with the CFIS Point Spread Function (PSF)
- Combination of the deflector and the lensed source images

Let's go deeper into details about the different steps and the assumption and choices made during the process. First assumption is the assignation of a mass profile model. The model used is the singular Isothermal Ellipsoid (SIE) model; a generalization of the singular isothermal sphere discussed in the section 1.1.3. This model is parameterized by five free parameters: Einstein radius, center coordinates of the lens, ellipticity and position angle. Since every image was design to host the deflector center at the center of the image, the center coordinates is a fixed value. The ellipticity and the position angle (PA) were derived from the second moment of the light profile of the LRG. In this model it is assumed that the ellipticity and the PA derived from the light distribution is the same as the mass distribution profile.

This being done, a source galaxy is randomly selected within the HST sample. with the redshift information of both galaxies and the velocity dispersion the Einstein radius is computed. The value of Einstein radius is imposed to fall in the interval $0.8" < R_E < 3.0"$. The lower limit is chosen to prevent lens-galaxy blending while the upper limit is set to fit into the image frame. If those conditions are not met, another source galaxy is chosen until it fits. After 100 iteration the velocity speed of

the deflector is increased by 50%. If the conditions are not met after all this process, the deflector is discarded from the dataset. As explained in the paper [14], This velocity dispersion boost involve few objects with small velocity dispersion and it is not expected to introduce a significant morphological bias.

The next systematic choice made during the building process is the total magnification constraint. They decided to impose $\mu \geq 2$ because it coincide with the threshold for a multiple image lens. Setting a higher limit would have increase the number of Einstein rings among the simulations and this could lead to an increase of false positives by mistaking ring galaxies.

When all those conditions are met, a high resolution image of the lensed source is computed and convolved with the CFIS PSF. Here the HST Point spread function is neglected since it iis sharper than the CFIS PSF. But before applying the CFIS PSF, it is important to re-sample the PSF to the HST pixel size and then down-sampled to the CFIS pixel size after the convolution. The final step is the addition of the lensed source image to to lens galaxy image.

2.2 Exploration of the dataset

Our dataset is made of multiple files divided into 5 type of data. We have first `LRG only` images which are the CFIS-r images as the fig 2.1. The second type of images are `Lensed source only` images which are the lensed images of a HST source galaxy. In fig 2.2. The third photometric-based images are the combination of `LRG only` and `Lensed source only` images which gives `Lens simulation` images. You could find in fig 2.3 those images which is the combination of images in fig 2.1 and 2.2. The two other type of data are PSF and RMS files. PSF files contains the two dimensional function associated to the response of a focused imaging system (here the Canada France Hawaii Telescope) to a point source. By inverse convolution we cancel the systematic effects implied by the Telescope. We only get the PSF from CFHT but as mentioned in section 2.1 we neglected the HST PSF. Finally, RMS files correspond to Root Mean Square errors associated to each pixels. RMS files were built from weight maps computed from gain and relative normalisation of noise using `SWarp`[4] software. It is important to note that we only get RMS files associated with `LRG only` images. We will see later how to generate RMS files for `Lens simulation` files. A sample of PSF and RMS files can be found in figure 2.5.

[4] `https://www.astromatic.net/software/swarp/`

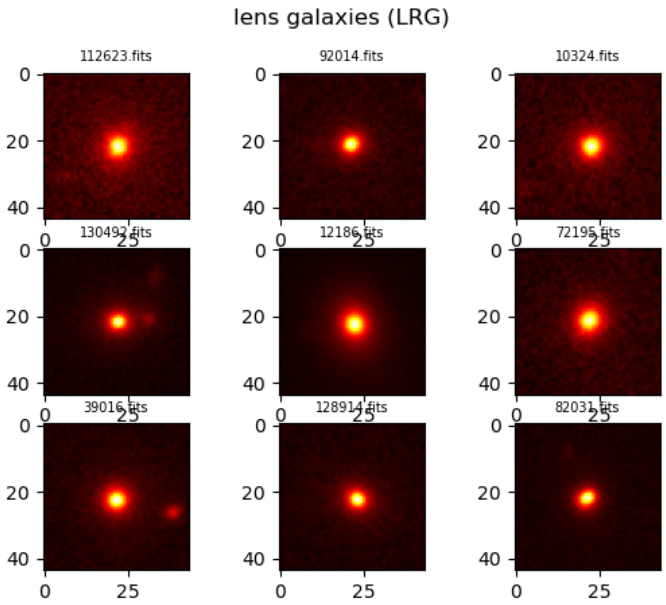

Fig. 2.1.: Sample of 9 images from the CFIS-r dataset. Those images are used as lens galaxies during the design of the dataset. Images are displayed with a red colormap and are not True color images

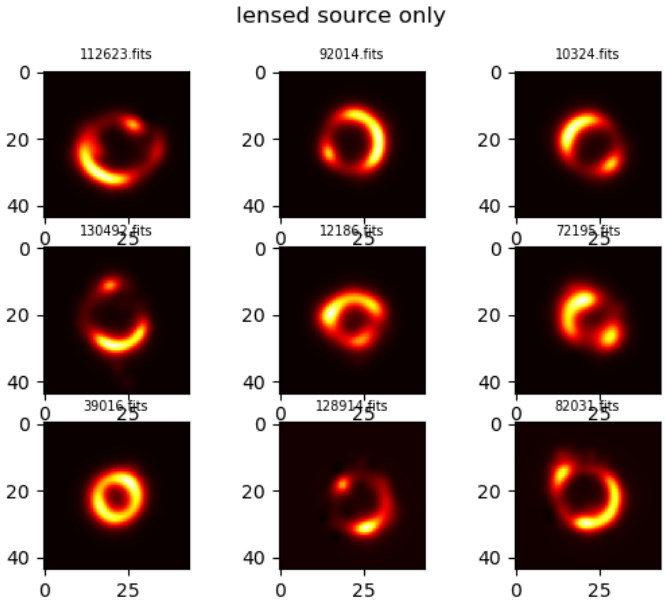

Fig. 2.2.: Sample of 9 simulated lens images from the HST source galaxies dataset. Those images are used as lens features during the design of the dataset. Images are simulated lenses according to lens galaxies displayed in fig 2.1.

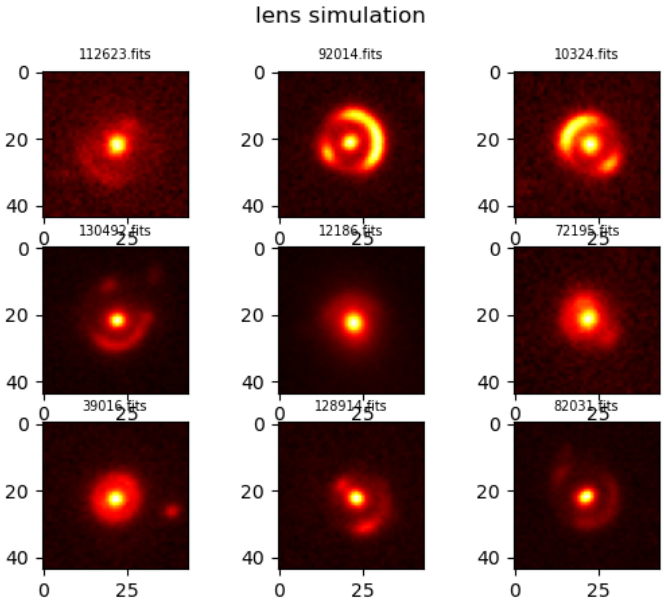

Fig. 2.3.: Sample of 9 simulated images from the CFIS-r and HST dataset. Those images are addition of fig 2.1 and 2.2 images.

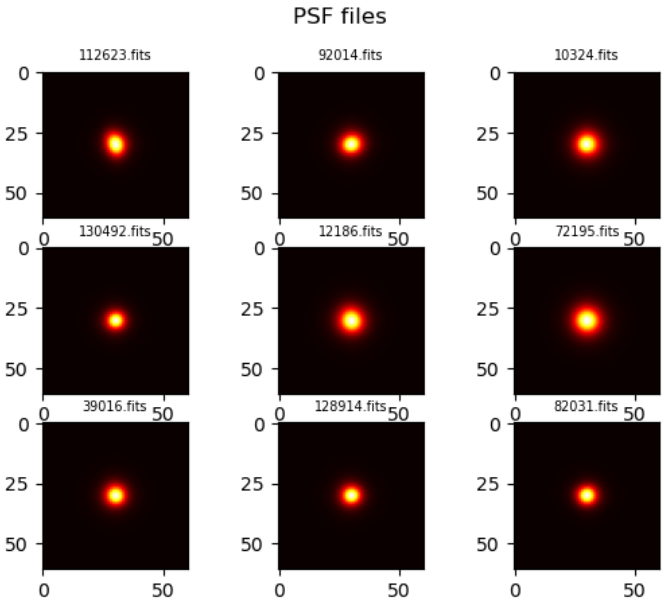

Fig. 2.4.: Sample of 9 PSF images from the Canada France Hawaii Telescope.

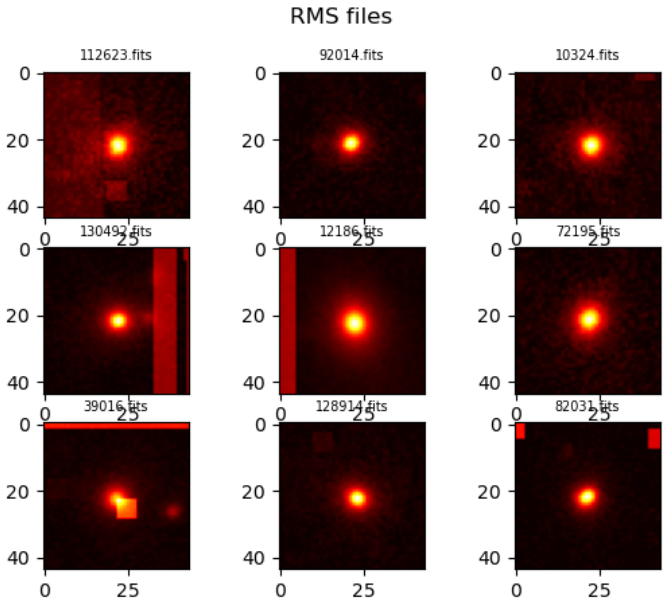

Fig. 2.5.: Sample of 9 RMS images associated with CFIS-r images. Squares on some images result from a mask of satellite tracks, cosmic rays or dead pixels.

2.3 Noise and signal

Imaging galaxies is not as simple as taking photograph as daily photography. Imaging deep sky objects implies low light intensity conditions and different noises becomes non-negligible. Those noises arise due to different physical phenomenon that we won't emphasize here because they have been corrected. However we will focus on the photonic noise which is persistent and important to quantify.

The photonic noise is linked to the physical nature of the light and affect detectors. This phenomenon is not perceptible by the human eye because of the retinal persistence that cancels irregularities in the photonic flux. For a given pixel cell, the amount of detected photons per time unit (photonic flux) is not a constant value. Thus, the amount of photons detected between neighbour cells will be different and the photonic noise arise. This noise is well quantified by the statistical law of Poisson. and we can evaluate the noise $\sigma_{photons}$ by the following equation, with N the number of detected photons:

$$\sigma_{photons} \propto \sqrt{N} \tag{2.1}$$

In our case, we can consider that the image is made of photons from the object of interest and photons coming from the background sky $I = I_{obj} + I_{sky}$. Pixels Intensities are expressed as ADU units which means Analog-to-Digital-Units and are link to Intensity in electron I_e units by the gain g.

$$I_{ADU} = I_e \times g \tag{2.2}$$

Thanks to equation 2.1, $I_e = \sigma_e^2 = RMS^2$ and we then get the following relation:

$$I_{ADU} = RMS^2 \times g \tag{2.3}$$

And the total Root Mean Square error is :

$$RMS^2 = \sigma_{obj}^2 + \sigma_{sky}^2 \approx \frac{I_{ADU}}{g} + \sigma_{sky}^2 \tag{2.4}$$

In order to verify that `LRG only` images are background subtracted and that our images are well calibrated, let's verify this linear relation by plotting pixel values as a function of RMS^2 as it can be found in fig 2.6. For low values of pixels it is easy to observe that the background noise is dominant and will lead to a plateau that is present in fig 2.6. If a mask is present in the RMS image we will have points away from the point cloud with the same profile but translated along y axis. An exemple is available in fig 2.7.

In order to check that images are well background substracted, we will neglect the plateau to get a more accurate fit on point cloud but we will also evaluate the background noise by only considering this plateau. A sample of 10 fit are displayed in fig 2.8 and values of the computed gain and computed σ_{sky}^2 are available in table 2.1. Fitted gain values are compared to the gain values available in the image headers. for the σ_{sky}^2 we compared fitted values with the value evaluated by tacking the mean value of the so called plateau. I also evaluated it by another method that I call the corner method. The corner method consists in taking some pixels values at the 4 corners of the image where the background is dominant. I took a square kernel of 5 pixels large at each corner so we have a total of 100 pixels. To obtain the background noise, I took the squared standard deviation of those pixels. We clearly see that gain values computed are coherent with the ones found in image headers and we also have same evaluations for the background noise. It is particularly true between the fit and the plateau method. However corner methods only consider 100 pixels which is a small sample of the total background sky and

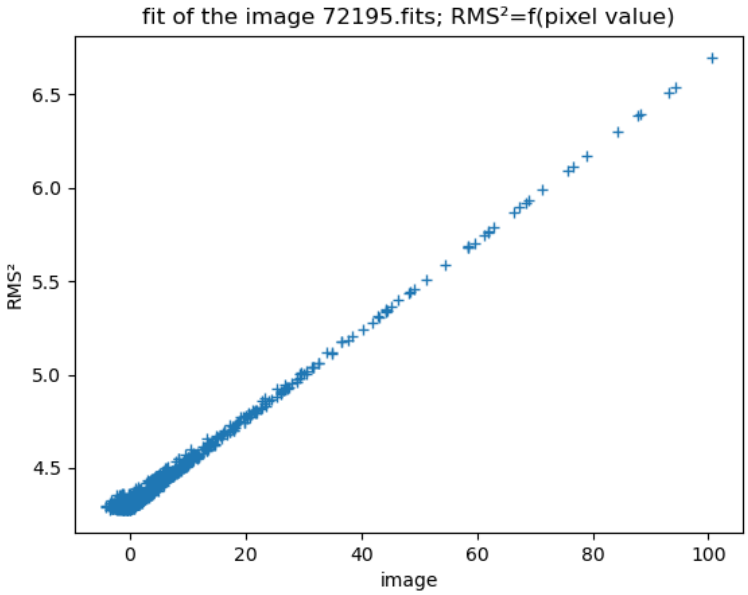

Fig. 2.6.: Pixel value in ADU as a function of RMS^2 for `LRG only` images

can thus under evaluate σ^2_{sky}. Moreover in the case of polluted images, there is a non-zero probability that the polluting source is located in the corner. Also, it does not take into account masks for cosmic rays, satellite tracks or dead pixels implying an error in the computation.

In the following, we will need RMS files for `Simulated images`, but we only have RMS files for `LRG only` images. Now that we know a bit more about the link between signal and the noise, it is easy to built a new RMS file for `Simulated images`. But before that I checked that images are a simple addition of `LRG only` and `Lensed source only` images by substracting both files from the simulated one. So based on equation 2.3, I reconstructed the RMS file with the quadratic sum of the already existing RMS file and a computed Mean Square error using the gain value available in the `LRG only` headers. Here is the expression of the new RMS:

$$RMS_{reconstructed} = \sqrt{RMS^2 + \frac{I_{ADU,Lensed_source_only}}{g_{LRG}}} \tag{2.5}$$

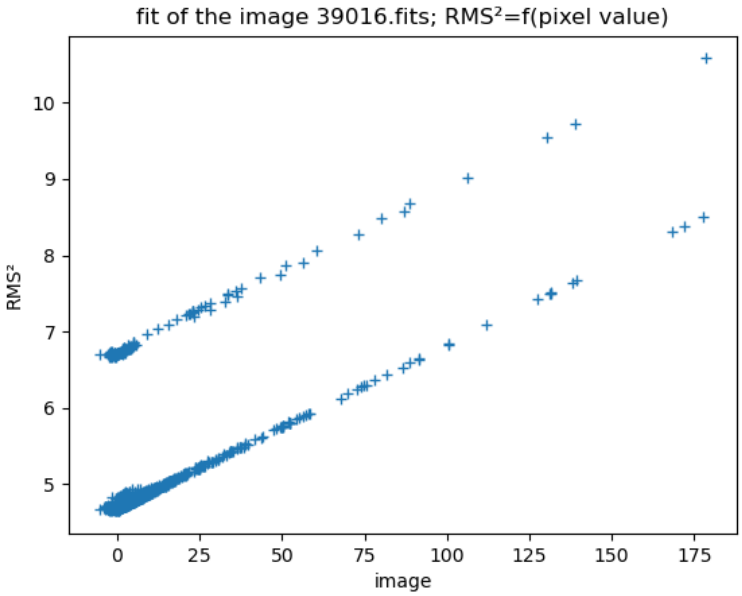

Fig. 2.7.: Pixel value in ADU as a function of RMS^2 for `LRG only` images with polluting source and RMS mask.

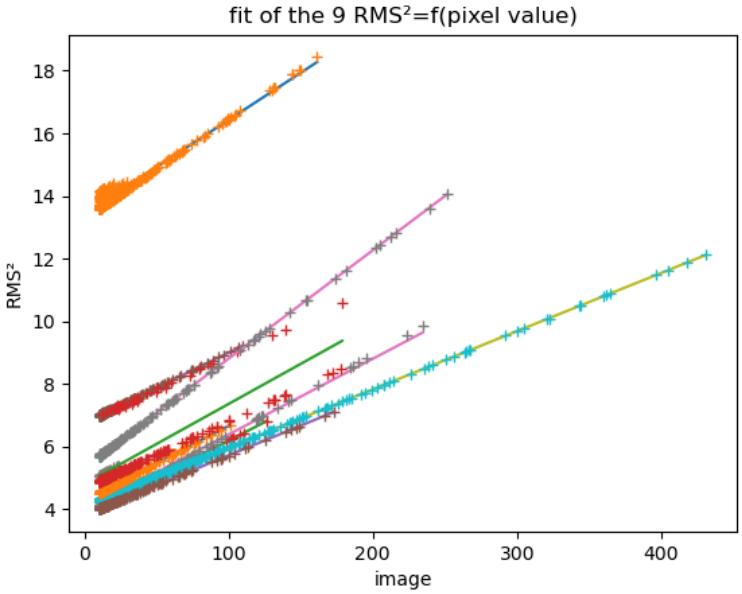

Fig. 2.8.: Linear regression of 9 `LRG only` images pixels from the CFIS-r as a function of RMS^2.

computed gain (fit)	real gain	σ^2_{sky} (fit)	σ^2_{sky} (plateau)	σ^2_{sky} (corner method)
33.27	31.58	13.43	13.56	12.12
42.36	42.36	3.84	3.88	3.19
44.79	44.49	6.77	6.81	4.00
41.43	39.04	3.98	4.11	2.72
53.92	53.97	4.12	4.58	9.35
42.12	41.83	4.29	4.35	3.73
39.16	46.55	4.82	4.86	2.78
52.78	52.75	3.83	3.88	3.53
28.93	29.03	5.36	5.48	4.16

Tab. 2.1.: Comparison of values computed for the gain and the background noise. fit values stand for values computed thanks to linear regression, plateau by tacking the mean value of the plateau and corner method by the method described in section 2.3. The real gain is the one available in the image header.

Bibliography

[1] I. Newton, *Optiks or a Treatise of the Reflexions, Refractions, Inflexions Colours of Light*. 1704, Book 3, Part 1, Querie 1 (cit. on p. 1).

[2] R. McCormmach, "John michell and henry cavendish: Weighing the stars," vol. 4, no. 2, pp. 126–155, Dec.1968 (cit. on p. 1).

[3] K.-H. Lotze and S. Simionato, "Henry Cavendish and the effect of gravity on propagation of light: A postscript," *The European Physical Journal H*, vol. 46, no. 1, p. 24, Sep. 2021 (cit. on p. 1).

[4] Wikisource. "Translation:on the deflection of a light ray from its rectilinear motion — wikisource." [Online; accessed 7-November-2022]. (2021), [Online]. Available: `https://en.wikisource.org/w/index.php?title=Translation:On_the_Deflection_of_a_Light_Ray_from_its_Rectilinear_Motion&oldid=10821714` (cit. on p. 1).

[5] A. Einstein. "On the influence of gravitation on the propagation of light." [Online; accessed 7-November-2022]. (1911), [Online]. Available: `https://einsteinpapers.press.princeton.edu/vol3-trans/393` (cit. on p. 1).

[6] J.-M. Ginoux, "Albert einstein and the doubling of the deflection of light," *Foundations of Science*, vol. 27, pp. 1–22, Feb. 2021 (cit. on p. 1).

[7] E. S. A. Dyson Frank Watson and D. C., "Ix. a determination of the deflection of light by the sun's gravitational field, from observations made at the total eclipse of may 29, 1919," *Philosophical Transactions of the Royal Society of London.*, vol. Series A, Containing Papers of a Mathematical or Physical Character, no. 220, pp. 291–333, 1920 (cit. on p. 1).

[8] F. Zwicky, "Nebulae as gravitational lenses," *Phys. Rev.*, vol. 51, pp. 290–290, 4 Feb. 1937 (cit. on pp. 1, 9).

[9] R. C. C. Dennis Walsh and R. Weymann, "0957 + 561 a, b: Twin quasistellar objects or gravitational lens?" *Nature*, vol. 279, pp. 381–384, 1979 (cit. on p. 1).

[10] T. York, N. Jackson, I. W. A. Browne, *et al.*, "CLASS B0631+519: last of the Cosmic Lens All-Sky Survey lenses,", vol. 361, no. 1, pp. 259–271, Jul. 2005. arXiv: `astro-ph/0505093 [astro-ph]` (cit. on p. 8).

[11] Y. Tsapras, "Microlensing searches for exoplanets," *Geosciences*, vol. 8, no. 10, p. 365, Sep. 2018 (cit. on p. 9).

[12] S. Rezaei, J. P. McKean, M. Biehl, W. de Roo, and A. Lafontaine, "A machine learning based approach to gravitational lens identification with the International LOFAR Telescope," *Monthly Notices of the Royal Astronomical Society*, vol. 517, no. 1, pp. 1156–1170, Nov. 2022 (cit. on p. 9).

[13]J. Pearson, C. Pennock, and T. Robinson, “Auto-detection of strong gravitational lenses using convolutional neural networks,” en, *Emergent Scientist*, vol. 2, p. 1, 2018, Publisher: EDP Sciences (cit. on p. 9).

[14]E. Savary, K. Rojas, M. Maus, *et al.*, “A search for galaxy-scale strong gravitational lenses in the Ultraviolet Near Infrared Optical Northern Survey (UNIONS),” Tech. Rep., Oct. 2021, Publication Title: arXiv e-prints ADS Bibcode: 2021arXiv211011972S Type: article (cit. on pp. 9–11, 13).

[15]J. L. Sérsic, “Influence of the atmospheric and instrumental dispersion on the brightness distribution in a galaxy,” *Boletin de la Asociacion Argentina de Astronomia La Plata Argentina*, vol. 6, pp. 41–43, Feb. 1963 (cit. on p. 10).

List of Figures

1.1 Deflection of light coming from a distant source (S) in the vicinity of a massive object (Lens: L) seen by the observer (O). 2
1.2 Analog situation of light traveling in vacuum from a distant source and propagating through a medium of refraction index n_ϕ. 3
1.3 Scheme of the general situation of a gravitational lens 4
1.4 Illustration of a gravitational lens with magnification. β correspond to the angle between deflector and source which is θ_s in the previous demonstration.θ_- and θ_+ are respectively the demagnified and magnified images positions. The dotted circle correspond to the Einstein ring position. 8

2.1 Sample of 9 images from the CFIS-r dataset. Those images are used as lens galaxies during the design of the dataset. Images are displayed with a red colormap and are not True color images 14
2.2 Sample of 9 simulated lens images from the HST source galaxies dataset. Those images are used as lens features during the design of the dataset. Images are simulated lenses according to lens galaxies displayed in fig 2.1. 14
2.3 Sample of 9 simulated images from the CFIS-r and HST dataset. Those images are addition of fig 2.1 and 2.2 images. 15
2.4 Sample of 9 PSF images from the Canada France Hawaii Telescope. . . 15
2.5 Sample of 9 RMS images associated with CFIS-r images. Squares on some images result from a mask of satellite tracks, cosmic rays or dead pixels. 16
2.6 Pixel value in ADU as a function of RMS^2 for `LRG only` images 18
2.7 Pixel value in ADU as a function of RMS^2 for `LRG only` images with polluting source and RMS mask. 19
2.8 Linear regression of 9 `LRG only` images pixels from the CFIS-r as a function of RMS^2. 19

List of Tables

2.1 Comparison of values computed for the gain and the background noise. fit values stand for values computed thanks to linear regression, plateau by tacking the mean value of the plateau and corner method by the method described in section 2.3. The real gain is the one available in the image header. 20

A.1 This is a caption text. 29
A.2 This is a caption text. 30

List of Listings

Example Appendix

A

Hello, here is some text without a meaning. This text should show what a printed text will look like at this place. If you read this text, you will get no information. Really? Is there no information? Is there a difference between this text and some nonsense like “Huardest gefburn”? Kjift – not at all! A blind text like this gives you information about the selected font, how the letters are written and an impression of the look. This text should contain all letters of the alphabet and it should be written in of the original language. There is no need for special content, but the length of words should match the language.

A.1 Appendix Section 1

This is the second paragraph. Hello, here is some text without a meaning. This text should show what a printed text will look like at this place. If you read this text, you will get no information. Really? Is there no information? Is there a difference between this text and some nonsense like “Huardest gefburn”? Kjift – not at all! A blind text like this gives you information about the selected font, how the letters are written and an impression of the look. This text should contain all letters of the alphabet and it should be written in of the original language. There is no need for special content, but the length of words should match the language.

Alpha	Beta	Gamma
0	1	2
3	4	5

Tab. A.1.: This is a caption text.

A.2 Appendix Section 2

And after the second paragraph follows the third paragraph. Hello, here is some text without a meaning. This text should show what a printed text will look like

at this place. If you read this text, you will get no information. Really? Is there no information? Is there a difference between this text and some nonsense like “Huardest gefburn”? Kjift – not at all! A blind text like this gives you information about the selected font, how the letters are written and an impression of the look. This text should contain all letters of the alphabet and it should be written in of the original language. There is no need for special content, but the length of words should match the language.

Alpha	Beta	Gamma
0	1	2
3	4	5

Tab. A.2.: This is a caption text.

After this fourth paragraph, we start a new paragraph sequence. Hello, here is some text without a meaning. This text should show what a printed text will look like at this place. If you read this text, you will get no information. Really? Is there no information? Is there a difference between this text and some nonsense like “Huardest gefburn”? Kjift – not at all! A blind text like this gives you information about the selected font, how the letters are written and an impression of the look. This text should contain all letters of the alphabet and it should be written in of the original language. There is no need for special content, but the length of words should match the language. Hello, here is some text without a meaning. This text should show what a printed text will look like at this place. If you read this text, you will get no information. Really? Is there no information? Is there a difference between this text and some nonsense like “Huardest gefburn”? Kjift – not at all! A blind text like this gives you information about the selected font, how the letters are written and an impression of the look. This text should contain all letters of the alphabet and it should be written in of the original language. There is no need for special content, but the length of words should match the language.

Colophon

This thesis was typeset with LaTeX 2_ε. It uses the *Clean Thesis* style developed by Ricardo Langner. The design of the *Clean Thesis* style is inspired by user guide documents from Apple Inc.

Download the *Clean Thesis* style at `http://cleanthesis.der-ric.de/`.

Declaration

You can put your declaration here, to declare that you have completed your work solely and only with the help of the references you mentioned.

, June 2023

Laisney Clément